HHS Public Access

Author manuscript

Cell Rep. Author manuscript; available in PMC 2024 February 06.

Published in final edited form as:

Cell Rep. 2023 March 28; 42(3): 112159. doi:10.1016/j.celrep.2023.112159.

Opposing retrograde and astrocyte-dependent endocannabinoid signaling mechanisms regulate lateral habenula synaptic transmission

Nathan D. Winters[1,2], **Veronika Kondev**[2,3], **Niharika Loomba**[3], **Eric Delpire**[3,4,5], **Brad A. Grueter**[1,2,3,4,5], **Sachin Patel**[6,7,*]

[1]Department of Pharmacology, Vanderbilt University School of Medicine, Nashville, TN 37232, USA

[2]Vanderbilt Center for Addiction Research, Vanderbilt University School of Medicine, Nashville, TN 37232, USA

[3]Vanderbilt Brain Institute, Vanderbilt University School of Medicine, Nashville, TN 37232, USA

[4]Department of Anesthesiology, Vanderbilt University School of Medicine, Nashville, TN 37232, USA

[5]Department of Molecular Physiology and Biophysics, Vanderbilt University School of Medicine, Nashville, TN 37232, USA

[6]Northwestern Center for Psychiatric Neuroscience, Department of Psychiatry and Behavioral Sciences, Feinberg School of Medicine, Northwestern University, Chicago, IL 60611, USA

[7]Lead contact

SUMMARY

The lateral habenula (LHb) encodes aversive states, and its dysregulation is implicated in neuropsychiatric disorders, including depression. The endocannabinoid (eCB) system is a neuromodulatory signaling system that broadly serves to counteract the adverse effects of stress; however, CB_1 receptor signaling within the LHb can paradoxically promote anxiogenic- and depressive-like effects. Current reports of synaptic actions of eCBs in the LHb are conflicting and lack systematic investigation of eCB regulation of excitatory and inhibitory transmission. Here, we report that eCBs differentially regulate glutamatergic and GABAergic transmission in the LHb, exhibiting canonical and circuit-specific inhibition of both systems and an opposing potentiation of synaptic glutamate release mediated via activation of CB_1 receptors on astrocytes.

*Correspondence: sachin.patel@northwestern.edu.

AUTHOR CONTRIBUTIONS

N.D.W., V.K., and N.L. conducted all experiments and analyzed the data in the laboratories of B.A.G and S.P. N.D.W., B.A.G., and S.P. contributed to experimental design. E.D. generated *Cnr1* floxed mice. N.D.W. and S.P. are responsible for study conception and data interpretation. N.D.W., B.A.G., and S.P wrote the manuscript.

DECLARATION OF INTERESTS

S.P. is a scientific consultant for Psy Therapeutics, Janssen Pharmaceuticals, and Jazz Pharmaceuticals unrelated to the present work.

SUPPLEMENTAL INFORMATION

Supplemental information can be found online at https://doi.org/10.1016/j.celrep.2023.112159.

Moreover, simultaneous depression of GABA and potentiation of glutamate release increases the net excitation-inhibition ratio onto LHb neurons, suggesting a potential cellular mechanism by which cannabinoids may promote LHb activity and subsequent anxious- and depressive-like aversive states.

Graphical Abstract

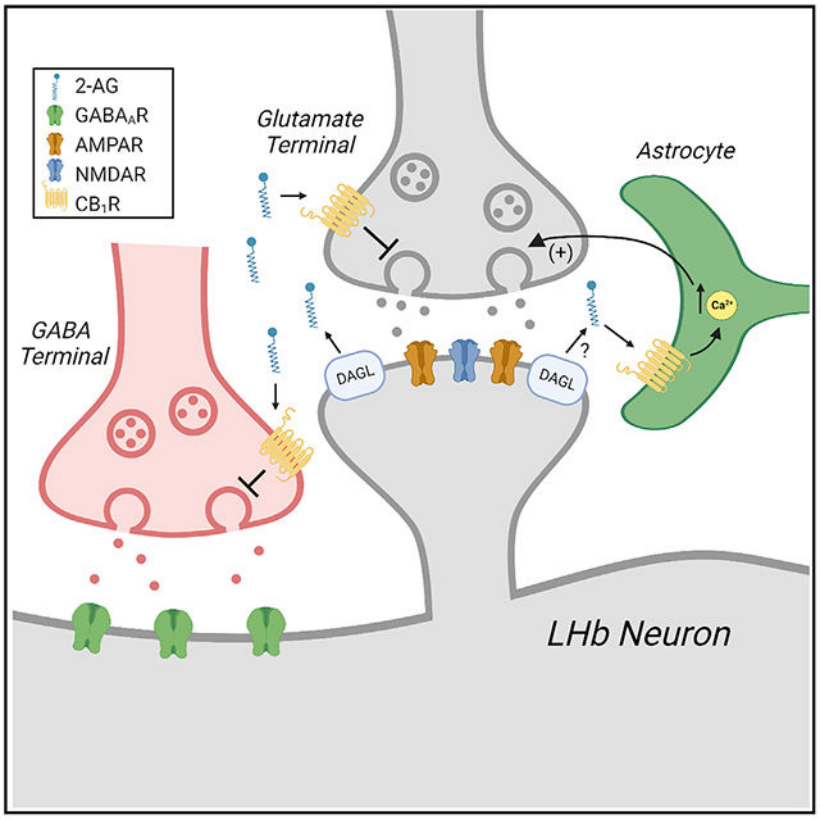

In brief

Winters et al. report differential endocannabinoid modulation of lateral habenula (LHb) synaptic transmission and describe divergent control over excitatory vs. inhibitory transmission and over distinct inputs to the LHb. Furthermore, they find astrocytic CB_1 receptors potentiate LHb glutamate release and contribute to how endocannabinoids regulate net synaptic drive onto LHb neurons.

INTRODUCTION

The lateral habenula (LHb) is a conserved epithalamic brain structure critical in guiding behavioral responses to aversive stimuli. Serving as an integrative hub between the forebrain and midbrain monoaminergic nuclei, the LHb regulates diverse physiological and behavioral functions.[1] Activation of the LHb is generally aversive and plays an increasingly evident role in neuropsychiatric disease, particularly in depression.[2] Despite this, the molecular systems orchestrating synaptic activity within the LHb are poorly understood. One system of

particular interest is the endocannabinoid (eCB) system, as it strongly controls synaptic signaling in other brain areas[3] and is heavily implicated in the etiology of affective disorders.[4]

The eCB system is a lipid-derived retrograde signaling system that generally functions to suppress presynaptic neurotransmitter release. It is comprised of type 1 and 2 cannabinoid receptors (CB_1 and CB_2), the two major eCB ligands (2-arachidonoylglycerol [2-AG] and anandamide [AEA]), and their biosynthetic and degradative enzymes. In the LHb, CB_1 receptors are present on excitatory and inhibitory terminals, postsynaptic neuronal membranes, mitochondria, and astrocytic membranes.[5] Intra- LHb CB_1 activation promotes depressive- and anxiety-like phenotypes in rats, whereas CB_1 blockade exerts anxiolytic- and antidepressant-like effects.[5] How these divergent phenotypes are produced remains a major open question in the field, as eCB manipulations in the LHb produce phenotypes opposite to those elicited by systemic or corticolimbic eCB signaling, which generally promotes anxiolysis and stress resiliency.[6-9] Reports of eCB actions at LHb synapses are conflicting and do not adequately account for these observations. For example, eCBs have been shown to inhibit both GABA and glutamate release under some conditions,[10,11] which would be predicted to have anxiogenic and anxiolytic effects, respectively. These observations highlight the need for systematic interrogation of eCB function at glutamatergic and GABAergic synapses in the LHb to provide insight into potential cellular mechanisms subserving the paradoxical aversive nature of eCBs in the LHb.

Using electrophysiology and pharmacology in acute brain slices, here we report opposing synaptic and astrocytic mechanisms by which eCBs differentially regulate LHb synaptic transmission. While we find circuit-specific canonical cannabinoid-mediated inhibition of evoked glutamate and GABA onto LHb neurons, our data uncover an astrocyte-dependent CB_1 mechanism potentiating spontaneous glutamate release. Collectively, our data identify opposing mechanisms of direct synaptic depression and indirect synaptic potentiation via eCB signaling in astrocytes, which may promote net LHb activity and potentially explain the pro-depressive effects of LHb CB_1 signaling. Furthermore, given the role of the LHb in depressive disorders, these findings may have broad implications for the cellular mechanisms underlying cannabinoid-associated depression[12] and the aversive effects of high-dose cannabinoids.[13,14]

RESULTS

eCBs differentially regulate glutamatergic and GABAergic synapses in the LHb

To assess eCB functionality at excitatory and inhibitory synapses in the LHb, we utilized patch-clamp electrophysiology in acute *ex vivo* brain slices. Holding neurons near the reversal potentials for glutamate and GABA allowed for electrical isolation of both spontaneous excitatory and inhibitory postsynaptic currents (sEPSCs and sIPSCs, respectively) from single LHb neurons (Figure 1A). Electrically isolated currents were predominantly glutamatergic or GABAergic, respectively (Figures S1A and S1B), without significant contribution by glycine receptors[15,16] (Figure S1C). Incubation of brain slices in the cannabinoid receptor agonist CP55,940 unexpectedly increased sEPSC frequency and amplitude (Figures 1B and 1C). In line with this, both the CB_1 inverse agonist rimonabant

(Rim) and the diacylglycerol lipase inhibitor DO34 significantly reduced sEPSC frequency (Figures 1B and 1C), suggesting the presence of a tonic positive modulatory 2-AG-CB_1 tone on spontaneous glutamate release. The monoacylglycerol lipase inhibitor JZL184 had no effect on sEPSC frequency or amplitude (Figures 1B and 1C). CP55,940 significantly reduced sIPSC frequency and amplitude (Figures 1D and 1E), in line with canonical eCB actions at GABAergic synapses and in agreement with Authement et al.[10] None of the other compounds tested had a significant effect on sIPSC frequency or amplitude (Figures 1D and 1E). Rim also had no effect on pharmacologically isolated sIPSCs measured at −70 mV (Figure S1D). When examining the sEPSC/sIPSC frequency ratio within cell, we found that CP55,940 significantly increased the excitation-inhibition (E/I) ratio onto LHb neurons, with no other compound exhibiting a significant effect on this measure (Figure 1F). These data suggest a differential role for 2-AG-CB_1 signaling at excitatory vs. inhibitory synapses with a shunting toward enhanced E/I ratio.

Contrasting our sEPSC data, it has been shown that CB_1 receptors inhibit evoked glutamate release in the LHb[11,17]; however, cannabinoid effects on evoked GABAergic transmission are not known. We therefore next examined the effects of cannabinoid receptor activation on evoked GABA release onto LHb neurons. We found that bath application of CP55,940 significantly reduced evoked IPSC (eIPSC) amplitude and caused a non-significant increase in the coefficient of variation (CV), another index of presynaptic release probability (Figures S1E-S1G), confirming that evoked GABA release is also inhibited by cannabinoid receptors. We next assessed activity-dependent engagement of eCB signaling at LHb synapses by measuring depolarization-induced suppression of excitation or inhibition (DSE or DSI, respectively). DSE/I are a electrophysiological methods for eliciting phasic eCB release and short-term plasticity wherein brief depolarization of the postsynaptic cell triggers Ca^{2+} entry that results in the synthesis and retrograde release of 2-AG to depress neurotransmitter release via presynaptic CB_1 receptors.[3,18] For evoked EPSCs (eEPSCs), we found that 10 s depolarization to +30 mV resulted in minimal effect on eEPSC amplitude. In contrast, depolarization to +30 mV resulted in a significant transient depression of eIPSC amplitude (Figures 1G and 1H), and this effect was blocked by Rim (Figures 1H and S1H). This presence of DSI, but not DSE, at LHb synapses further supports our spontaneous transmission data that suggest that the LHb eCB system exerts stronger inhibition of GABAergic transmission and thus may serve to promote net synaptic excitation of LHb neurons.

Given the diverse distribution of CB_1 immunoreactivity in the rodent LHb, including postsynaptic and mitochondrial compartments,[5] we also probed for potential effects of CB_1 activation on LHb neuron excitability. CP55,940 incubation had no effect on the number of action potentials fired in response to square-wave current injection (Figure S1I) and had no effect on resting membrane potential, input resistance, or tonic firing frequency in a cell-attached configuration (Figures S1J-S1L). These data suggest that the effects of CB_1 activation in the LHb are likely restricted to modulation of synaptic neurotransmitter release.

Distinct inputs to the LHb are differentially regulated by eCBs

While previous studies have demonstrated that cannabinoid receptors can depress electrically evoked glutamate release onto LHb neurons,[11,17] our data showing potentiation of sEPSCs suggest that distinct afferents to the LHb may be under divergent control of eCB signaling. To address this possibility, we utilized optogenetic projection targeting to isolate two distinct LHb inputs, the lateral preoptic area (LPO) and the entopeduncular nucleus (EPN). These inputs send dual-component excitatory-inhibitory projections to the LHb are generally aversive when activated and have been implicated in behavioral states relevant to disease pathology.[19-21] We first examined eCB regulation of the LPO input, a hypothalamic structure that sends glutamate and GABA projections to the LHb via separate populations of neurons.[19] To target LPO synapses, we injected mice in the LPO with AAV5-CaMKIIa-ChR2(H134R)-EYFP and pharmacologically isolated optically evoked EPSCs and IPSCs (oEPSCs and oIPSCs, respectively) in the LHb (Figure 2A). Examining the glutamatergic LPO-LHb circuit, we found robust depression of oEPSC amplitude upon bath application of CP55,940 (Figures 2B and 2C). There was no effect on the paired-pulse ratio (PPR) or CV (Figure 2D). With regards to the GABAergic LPO-LHb circuit, we found depression of oIPSC amplitude upon CP55,940 application (Figures 2B and 2E), as well as an increase in the PPR and non-significant increase in the CV (Figure 2F). These data suggest that the LPO-LHb circuit is regulated by cannabinoid receptors, with stronger relative control of the glutamate input (Figure S2A). To probe tonic and phasic eCB regulation of this circuit, we examined the effects of Rim on release probability by delivering a 250 ms pulse train at 20 Hz and by analysis of DSE/I. At the glutamate LPO input, Rim accelerated synaptic depression of oEPSC amplitude, indicative of increased release probability (Figure 2G) and revealing tonic CB_1 inhibition of LPO-LHb glutamatergic transmission. This contrasts our sEPSC data but is in line with canonical retrograde synaptic eCB mechanisms. With regards to phasic 2-AG release, our DSE protocol did not detect DSE at the LPO-LHb circuit (Figure 2H). At the GABAergic LPO input, Rim had no effect on presynaptic release probability, and we did not detect DSI (Figures 2I and 2J).

We next examined eCB regulation of the EPN input, a basal ganglia structure that sends a dual-component projection wherein glutamate and GABA are released from the same terminals.[21] To do this, we injected AAV5-Ef1a-DIO-ChR2-EYFP into the EPN of somatostatin-Cre (SST-IRES-Cre) mice (Figure 2K). This approach selectively targets the SST + glutamate/GABA co-releasing neurons of the EPN and avoids a distinct excitatory EPN-LHb circuit.[22] We found that bath application of CP55,940 had no significant effect on oEPSC or oIPSC amplitude or any other release measure examined except for a small but significant increase in the glutamate PPR (Figures 2L-2P and S2B). Furthermore, Rim had no effect on release probability of glutamate or GABA, and CB_1-sensitive DSE/DSI were absent at this input (Figures 2Q-2T). These data provide evidence for circuit specificity in eCB modulation of LHb synapses and identify that the LPO input is inhibited by canonical synaptic eCB mechanisms. These data further support previous data showing cannabinoid inhibition of evoked glutamate release[11,17] and, together with our sEPSC data, suggest that there may be opposing eCB mechanisms that can inhibit or potentiate synaptic glutamate release in distinct contexts.

Astrocytic CB_1 receptors positively modulate LHb glutamate release

We next sought to further investigate the opposing effect of CB_1 receptor activation on spontaneous vs. evoked glutamatergic transmission and probed the mechanisms underlying the potentiating effects of eCB signaling on sEPSCs seen in Figure 1B. We first sought to exclude the possibility of indirect network effects due to the lack of synaptic blockers in these earlier experiments. We repeated the Rim and DO34 experiments in the presence of the $GABA_A$ receptor blocker picrotoxin, as well as the $GABA_B$ receptor antagonist CGP 54626. As shown before, blockade of the 2-AG-CB_1 axis by Rim or DO34 significantly reduced sEPSC frequency (Figure S3A), confirming that these findings are not related to indirect effects of GABAergic transmission. To probe the reversibility of this mechanism, we next treated all slices with DO34 to deplete constitutive 2-AG signaling to determine if cannabinoid receptor activation by an exogenous agonist could restore the reduced glutamate release observed in this condition. Indeed, CP55,940 significantly enhanced sEPSC frequency in DO34-treated slices relative to slices treated with DO34 alone (Figure S3B), confirming the bidirectionality of this potentiating 2-AG-CB_1 tone.

One mechanism by which eCBs have been reported to enhance synaptic transmission is via CB_1 signaling in astrocytes. A growing body of literature has demonstrated that astrocytes express CB_1 receptors that couple to intracellular Ca^{2+} mobilization and subsequent gliotransmission, which can modulate synaptic release.[23-27] Supporting this hypothesis, astrocyte membranes exhibit the highest relative density of CB_1 receptor immunoreactivity in the rodent LHb.[5] To determine whether LHb astrocytic CB_1 receptors were functional, we monitored astrocyte Ca^{2+} signals as a functional readout for these receptors from mice generated to genetically encode the Ca^{2+} indicator GCaMP6f selectively in astrocytes (Aldh1l1-Cre/ERT2:Ai95D) (Figure 3A). In *ex vivo* brain slices from these mice, we delivered a local pressure pulse application of CP55,940 to examine local Ca^{2+} responses (Figure 3B). Application of CP55,940 resulted in a time-locked local elevation in bulk fluorescent Ca^{2+} signals near the site of drug application, and this effect was blocked by the CB_1 antagonist NESS-0327 (Figure 3C), confirming the selectivity of CB_1 receptors in mediating this effect. These data support previous reports of astrocytic CB_1 coupling to intracellular Ca^{2+} signaling in other brain regions and confirm the presence of functional CB_1 receptors coupling to this mechanism in the LHb.

To directly test the hypothesis that astrocytic CB_1 receptors are involved in the tonic potentiation of glutamate release, we selectively deleted CB_1 receptors from LHb astrocytes by viral expression of Cre recombinase under the astrocytic glial fibrillary acidic protein (GFAP) promoter (AAV8-GFAP-Cre-mCherry) in the LHb of *Cnr1*$^{flx/flx}$ mice (Figures 3D and S3C). These mice express a floxed allele for the CB_1 receptor gene, which we have previously demonstrated exhibits functional CB_1 deletion in the presence of Cre.[8] Using this approach, we found again that Rim significantly reduced sEPSC frequency onto LHb neurons from animals injected with a control virus (AAV8-GFAP-GFP), but notably, this effect was absent in LHb neurons from slices expressing Cre (Figure 3E). Furthermore, neurons from the Cre-vehicle condition exhibited a significantly reduced sEPSC frequency relative to GFP-vehicle control slices (Figure 3E), suggesting that astrocytic CB_1 receptor deletion mimics and occludes the effect of Rim on sEPSC frequency. These data

demonstrate that the tonic 2-AG-CB_1 tone that maintains physiological glutamatergic tone is mediated through astrocytic CB_1 receptors. We further demonstrated the involvement astrocytic CB_1 receptors in potentiating LHb glutamate release by examining CP55,940-induced potentiation of sEPSCs following 2-AG depletion by DO34. We found that CP55,940 significantly potentiated sEPSC frequency onto LHb neurons from GFP-injected control mice as seen in Figure S3B, and this effect was absent in neurons from Cre-injected mice (Figure 3F). Injection of AAV9-hSynapsin-GFP-Cre to delete CB_1 receptors from LHb neurons did not occlude the Rim-induced reduction in sEPSC frequency, controlling for off-target viral leak into neurons and further demonstrating the astrocytic specificity of these effects (Figure S3D). Taken together, these data identify astrocytic CB_1 as the source for the tonic positive eCB regulation of LHb glutamate release and demonstrate that stimulation of these receptors can potentiate glutamate release under conditions of depleted 2-AG signaling. Moreover, astrocytic CB_1 deletion had no effect on group I metabotropic glutamate receptor (mGluR)-driven long-term depression of evoked glutamate release (Figure S3E), which has been shown to be eCB dependent.[11] Astrocytic CB_1 deletion also did not eliminate CP55,940-induced depression of eEPSCs (Figure S3F) or sIPSCs (Figure S3G), indicating that canonical cannabinoid-mediated synaptic depression does not require local astrocytic CB_1 and providing further support for distinct and opposing retrograde neuronal and astrocytic CB_1 signaling systems in the regulation of LHb glutamatergic transmission.

DISCUSSION

Increased LHb activity drives aversion, increases depressive-like behavioral phenotypes, and has been posited to contribute to the pathophysiology of psychiatric disorders including depression.[1] Elucidating neuromodulator mechanisms that influence LHb activity could reveal effective approaches for the treatment of mood and anxiety disorders. Here, we identify an astrocyte-dependent mechanism by which tonic 2-AG-CB_1 signaling potentiates spontaneous glutamatergic transmission onto LHb neurons. In contrast, eCB-CB_1-mediated suppression of evoked release and spontaneous GABAergic transmission occur via canonical retrograde synaptic mechanisms.[3] At a population level, CB_1 appears to shunt the LHb spontaneous synaptic E/I ratio toward greater net excitation via simultaneous reductions in spontaneous GABAergic and potentiation of spontaneous glutamatergic transmission. These CB_1-induced synaptic effects are predicted to increase LHb output, enhancing aversion and increasing anxiety- and depressive-like phenotypes. These data could thus explain the antidepressant- and anxiolytic-like effects of intra-LHb CB_1 receptor blockade,[5] which could reduce spontaneous excitatory drive onto LHb neurons via impairment in astrocytic 2-AG-CB_1 signaling. It is also well known that high doses of exogenous cannabinoids,[13] and 2-AG augmentation under some conditions,[28] can produce aversive and anxiogenic phenotypes in rodents and humans, and it is tempting to speculate that potentiation of LHb glutamatergic transmission via astrocytic CB_1 could contribute to these phenomena, particularly given recent evidence that astrocytic CB_1 receptors may contribute to the aversive properties of cannabinoids.[29] These data provide mechanistic insight into how eCB signaling within the LHb could produce aversive-like phenotypes and potentially contribute

to dose-dependent subjective experiences of exogenous cannabinoids, which have been thus far unexplained from a synaptic perspective.[14]

Astrocytic eCB signaling is a rapidly emerging area of interest,[30] spearheaded by seminal studies from Navarrete and Araque[24,25] that first identified functional CB_1 receptors on astrocytes in the hippocampus that coupled to intracellular Ca^{2+} mobilization and modulated local synaptic transmission. These findings have since been extended to numerous other brain areas.[23,26,27] Preceding our findings was the observation that the highest density of CB_1 receptor immunoreactivity in the rodent LHb is on astrocyte membranes,[5] although their functionality had not been determined. Our data demonstrate astrocyte CB_1 receptor functionality in the LHb and ascribe to them a function in the tonic potentiation of glutamate release to maintain physiological synaptic release probability. The mechanistic link between astrocytic CB_1 activation in the LHb and the potentiation of glutamate remains an open question. It is presumed that CB_1 mobilizes Ca^{2+} in astrocytes via coupling to G_q rather than canonical $G_{i/o}$ proteins due to a requirement for phospholi-pase C signaling and insensitivity to pertussis toxin,[24] although this remains to be definitively shown. CB_1-linked Ca^{2+} mobilization then leads to gliotransmitter release, and these mechanisms vary greatly by both brain region and synapse type under study and may involve multiple subcellular pools of CB_1.[31] For example, astrocytic CB_1 can potentiate synapses in the amygdala or hippocampus via stimulating astrocytic release of adenosine or glutamate, which facilitates synaptic release via presynaptic adenosine 2A or mGluR1, respectively.[23,25] Future studies should aim to identify whether similar or distinct molecular signaling mechanisms are recruited downstream of astrocytic CB_1 activation in the LHb.

Using optogenetic approaches, we also addressed whether eCB signaling in the LHb exhibits afferent specificity. Our studies reveal differential regulation of two inputs by eCBs, with the LPO synapses exhibiting depression by CB_1 activation and EPN synapses appearing insensitive to eCB modulation. Another important observation was the discrepancy between our circuit-specific eEPSC and sEPSC data with regards to the effects of CB_1 blockade. There are several potential explanations for this discrepancy: firstly, it is possible that the LPO and EPN are not the target inputs for regulation via astrocytic eCB mechanisms or are not major contributors to the spontaneously active synapse pool; secondly, studies reporting astrocytic CB_1 regulation of synaptic strength, including our own data, have relied on minimal stimulation or spontaneous transmission approaches.[23,25-27] Astrocytic eCB potentiation of glutamate release in the hippocampus is observed using minimal stimulation techniques but is not detectable when bulk stimulating larger numbers of synapses,[32] suggesting that there may be synaptic subpopulations amenable to astrocytic regulation and that are “lost in the noise” of our bulk stimulation methods; and lastly, there may be differential mechanisms regulating evoked and spontaneous neurotransmitter release in the LHb, as these modes of neurotransmission can exhibit molecularly distinct properties[33] and may be subject to regulation by differential eCB mechanisms. The degree to which highly synchronous release in the manner elicited by optogenetic approaches occurs *in vivo* is unknown, and thus the eCB signaling mechanisms that would predominate in a whole-animal model are difficult to predict conclusively. Future studies should address the relative contributions of canonical retrograde vs. astrocyte eCB signaling to LHb output and

determine the causal relationship between astrocytic CB_1-induced potentiation of glutamate release and the aversive nature of cannabinoids in the LHb.

In summary, we provide a framework for how eCBs modulate excitatory and inhibitory transmission in distinct cellular and synaptic contexts and provide a potential functional explanation for the aversive nature of CB_1 activation in the LHb,[5] which could occur via simultaneous depression of GABA and potentiation of glutamate via astrocytic CB_1 to enhance net synaptic excitation and promote LHb activity and depressive-like phenotypes.

Supporting this, chronically stressed rodents exhibit enhanced LHb neuron firing and elevated 2-AG content,[5] although acute stress may disrupt some forms of 2-AG mobilization at LHb glutamatergic synapses.[17] Selective targeting of LHb eCB signaling or astrocytic function could present new therapeutic targets for depression as well as substance use disorders, as LHb eCB signaling can also influence drug intake in a manner opposite to systemic modulation in some cases.[34,35] Finally, given the association between chronic cannabinoid use and depression[12] and the aversive effects of high-dose cannabinoids (e.g., THC),[13] these mechanisms may inform the importance of considering specific disease etiology for the application of cannabinoid-based therapeutics.

Limitations of the study

With regards to astrocytic CB_1 activation, our agonist incubation approach results in a high degree of variability (see Figures 3D and S3B), potentially originating from competition between presynaptic and astrocytic CB_1, so alternative methods for stimulating this mechanism may be appropriate for future studies. Importantly, given the time course of our incubation experiments, it cannot be ruled out that other non-gliotransmitter-mediated astrocyte mechanisms not yet linked to CB_1 activation may be involved, such as alterations in astrocyte glutamate clearance machinery, which can alter glutamate signaling in the LHb.[36]

We demonstrated that cannabinoid receptor-mediated reduction of sIPSC frequency was intact following astrocytic CB_1 deletion (Figure S3G) but did not explore basal phenotypes of astrocytic CB_1 receptor deletion on broader GABAergic transmission. We cannot rule out an interaction between astrocytic eCB signaling and inhibitory transmission, presenting a limitation in our model for the LHb eCB system.

Another limitation in our proposed model for the LHb eCB system is the unknown source for the tonic 2-AG tone that signals onto astrocyte CB_1. DO34 incubation terminates all DAGL activity in the slice, and astrocytes may produce 2-AG and signal onto local CB_1 receptors in an autocrine manner in culture.[37] Delineation of neuronal vs. astrocytic 2-AG production in distinct contexts will strengthen the model for interplay between these distinct eCB system components.

STAR★METHODS

RESOURCE AVAILABILITY

Lead contact—Further information and requests for resources and reagents should be directed to and will be fulfilled by the lead contact, Sachin Patel (sachin.patel@northwestern.edu).

Materials availability—This study did not generate new unique reagents.

Data and code availability

- All data reported in this paper will be shared by the lead contact upon request.
- This paper does not report original code.
- Any additional information required to reanalyze the data reported in this work paper is available from the lead contact upon request.

EXPERIMENTAL MODEL AND SUBJECT DETAILS

All experiments were approved by the Vanderbilt University Institutional Animal Care and Use Committees and were conducted in accordance with the National Institute of Health guidelines for the Care and Use of Laboratory Animals. 5–16 week-old male and female C57BL/6J mice obtained from Jackson Labs or bred in-house and were used for experiments throughout the manuscript. 10–18 week-old male and female *Cnr1*$^{flx/flx}$ mice bred in-house were used for experiments in Figure 3. Aldh1l1-Cre/ERT2 mice and Ai95D mice were obtained from Jackson Labs and crossed in-house to obtain Aldh1l1-Cre:Ai95D mice. 10–18 week-old male and female Aldh1l1-Cre:Ai95D mice were used for experiments in Figure 3. SOM-IRES-Cre mice and Ai14 mice were obtained from Jackson labs and crossed in-house to obtain SOM:Ai14 mice. 10–20 week-old male and female SOM:Ai14 mice were used for experiments in Figure 2. SOM:Ai14 mice were used over SOM-IRES-Cre mice due to the phenotype observed in homozygous SOM-IRES-Cre mice[39] and the availability of this line within our laboratory, as the Ai14 reporter construct should not interfere with our experimental strategy. Sex differences were not a primary analysis variable in this study and no overt sex differences were observed, thus all data are pooled from both sexes.

Generation of *Cnr1*$^{flx/flx}$ mice—See.[8]

METHOD DETAILS Surgeries

Mice were initially anesthetized with 5% isoflurane and then transferred to the stereotax (Kopf Instruments, Tujunga, CA) and kept under 2–3% isoflurane anesthesia. The hair over the incision cite was trimmed and the skin was prepped with alcohol and iodine scrub. The skull was exposed via a midline sagittal incision and treated with the local anesthetic, benzocaine (Medline Industries, Brentwood, TN), and a hole drilled in the skull above the injection site. For all surgeries, we used a motorized digital software (NeuroStar; Stoelting Co., Wood Dale, IL) to guide a 10 mL microinjection syringe (Hamilton Co., Reno, NV) driven by a Micropump Controller (World Precision Instruments, Sarasota, FL). Virus was delivered bilaterally into the LHb (AP −1.10, ML ±0.55, DV +2.95); LPO (AP +0.65,

ML ±0.52, DV +5.20) or EPN (AP −1.20, ML ±1.75, DV +4.70). All subjects received a 10 mg/kg ketoprofen (AlliVet, St. Hialeah, FL) injection as a perioperative analgesic, and additional post-operative treatment with ketoprofen was maintained for 48 h post-surgery.

***Ex vivo* electrophysiology—**For acute *ex vivo* brain slice preparation, mice were anesthetized using isoflurane, and transcardially perfused with ice-cold and oxygenated cutting solution consisting of (in mM): 93 N-Methyl-D-glucamine (NMDG), 2.5 KCl, 20 HEPES, 10 $MgSO_4 \cdot 7H_20$, 1.2 NaH_2PO_4, 30 $NaHCO_3$, 0.5 $CaCl_2 \cdot 2H_20$, 25 glucose, 3 Na-pyruvate, 5 ascorbic acid, and 5 N-acetylcysteine. Mice were then decapitated and brains collected. 200 μm coronal slices containing the lateral habenula were prepared on a vibrating Leica VT1000S microtome using standard procedures. Following collection of coronal sections, the brain slices were transferred to a 34°C chamber containing oxygenated cutting solution for a 10–20 min recovery period. Slices were then transferred to a 25°C holding chamber with solution consisting of (in mM): 92 NaCl, 2.5 KCl, 20 HEPES, 2 $MgSO_4 \cdot 7H_20$, 1.2 NaH_2PO4, 30 $NaHCO_3$, 2 $CaCl_2 \cdot 2H_20$, 25 glucose, 3 Na-pyruvate, 5 ascorbic acid, 5 N-acetylcysteine and were allowed to recover for ≥30 min. For recording, slices were placed in a perfusion chamber and continuously perfused with oxygenated artificial cerebrospinal fluid (ACSF; 31–33°C) consisting of (in mM): 113 NaCl, 2.5 KCl, 1.2 $MgSO_4 \cdot 7H_20$, 2.5 $CaCl_2 \cdot 2H_20$, 1 NaH_2PO_4, 26 $NaHCO_3$, 20 glucose, 3 Na-pyruvate, 1 ascorbic acid, at a flow rate of 2–3 mL/min. All drugs (except CNQX, D-AP5, and strychnine) were dissolved in DMSO and included in ACSF and holding/incubation chambers also containing 0.1–0.5 mg/mL BSA (except DO34). Drug concentrations for electrophysiology experiments (unless noted otherwise in figure legends) were (in μ5 CP55,940, 5 Rimonabant, 2.5 DO34, 1 JZL-184, 1 strychnine. Drug incubations were for a minimum of 30 min. For drug bath application experiments, cells were included in as data points in time course graphs provided they remained stable for a minimum of 15 min post-drug application, but were excluded from all other metrics if they did not remain stable the full time course. Slices incubated in CP55,940 or JZL-184 were used for <120 min so as to minimize potential effects of CB_1 desensitization. Equal volumes of DMSO were added to all vehicle solutions.

Lateral habenula neurons were identified at 40× magnification with an immersion objective with differential interference contrast microscopy. The majority of cells patched were in the medial ~2/3 of the lateral habenula due to the greater visibility and number of healthy cells in the slice, similar as previously reported.[40] All recordings (except cell-attached) were carried out in whole-cell configuration with borosilicate glass pipettes (2–6 MΩ). For spontaneous synaptic recordings, cells were voltage clamped at −70 or +20 mV with an intracellular solution containing (in mM): 120 Cs-gluconate, 2.9 NaCl, 5 tetraethylammonium-Cl, 20 HEPES, 2.5 Mg-ATP, 0.25 Na-GTP, 0.4 EGTA. Pharmacologically-isolated sIPSCs were recorded at −70 mV with an intracellular solution containing (in mM): 125 KCl, 4 NaCl, 10 HEPES, 4 Mg-ATP, 0.3 Na-GTP, and 10 Na-phosphocreatine. For evoked synaptic recordings cells were voltage clamped between −70-60 mV with an intracellular solution containing (in mM): 75 K-gluconate, 50 KCl, 4 NaCl, 10 HEPES, 4 Mg-ATP, 0.3 Na-GTP, 10 Na-phosphocreatine. 5 mM QX-314-Br was added fresh to internal aliquots for all voltage clamp experiments. Evoked or isolated

spontaneous glutamate recordings were carried out in the presence of the $GABA_A$ receptor blocker picrotoxin (50 μM). Evoked or isolated spontaneous GABA recordings were carried out in the presence of the AMPA receptor antagonist CNQX (10–20 μM) and NMDA receptor antagonist D-AP5 (50 μM). Electrical stimulation of synaptic currents was achieved by placing a stimulating electrode in the stria medullaris. Electrically-evoked postsynaptic currents were adjusted for a stable response baseline between ~100 and 500 pA. For current clamp recordings, baseline current was adjust to hold cells at −65 mV with an intracellular solution containing (in mM): 125 K-gluconate, 4 NaCl, 10 HEPES, 4 Mg-ATP, 0.3 Na-GTP, and 10 Na-phosphocreatine. For cell-attached recordings, pipettes were filled with extracellular ACSF solution. Silent neurons were not included in cell-attached datasets. Liquid junction potentials were not corrected for. For all experiments, cells were allowed to stabilize for ≥3 min following break-in and cells with a series resistance of ≤30 MΩ were included in analyses for voltage clamp experiments.

***Ex vivo* optogenetics—**For electrophysiological interrogation of the LPO-LHb circuit, WT C57 mice were bilaterally injected with 175–200 nL of AAV5-CaMKIIaChR2(H134R)-eYFP into the LPO. For the EPN circuit, SOM:Ai14 mice were bilaterally injected with 175–250 nL of AAV5-EF1a-DIO-hChR2(H134R)-EYFP-WPRE into the EPN. Optogenetic recordings of synaptic currents were obtained via 473 nm light stimulation (1–2 ms pulse width) using a Thorlabs LEDD1B T-Cube driver or CoolLED stimulation system. Light intensity was adjusted to achieve a stable response at submaximal (~40–80%) amplitude between ~100 and 2000 pA.

***Ex vivo* Ca^{2+} imaging—**Aldh1l1:Ai95D mice aged 5–10 weeks received 5 tamoxifen injections (75 mg/kg) 24 h apart. A minimum of 2 weeks for Cre induction and GCaMP6f expression was allowed before sacrificing for imaging experiments. *Ex vivo* brain slice preparation, recovery, and holding for Ca^{2+} imaging was performed as detailed above for electrophysiological experiments. Following recovery, 200 μm coronal slices containing the lateral habenula were transferred to the electrophysiology rig and perfused with ACSF (described above; 31–33°C) containing 0.5 mg/mL BSA to assist with drug solubility. Slices were imaged at 40X using a standard DIC widefield micro-cope and a Nikon DS-Qi2 camera. GCaMP6f fluorescence was imaged via excitation with a 473 nm LED using a Thorlabs LEDD1B T-Cube driver. Videos were recorded using NIS-Elements software (Nikon, Melville, NY) with constant illumination and a video frame rate of 1 frame per second. Pseudocolored heatmap images were generated from individual video frames in ImageJ.

Astrocytes in the lateral habenula were identified by their weak baseline GCaMP6f fluorescence and/or spontaneous Ca^{2+} activity. For local agonist application, CP55,940 was dissolved as an initial stock of 50 mM in DMSO, then diluted in ACSF containing 0.5 mg/mL BSA, for a final concentration of 100 μM CP55,940. This solution was loaded into patch pipettes connected to a Picospritzer III (Parker, Hollis, NH). For recordings, pipettes were maneuvered near identified cells at a distance of ~30–50 μm. A 30 s baseline was recorded before a 10 s pulse of CP55,940 was delivered (8–12 psi), followed by an additional 20 s of recovery. Mechanical agitation of visible blood vessels was avoided. For

antagonist experiments, the CB_1 receptor neutral antagonist NESS-0327 was used to negate the possibility of altered Ca^{2+} dynamics due to the inverse agonist properties of Rimonabant.

Immunohistochemistry and imaging—Mice were anesthetized using isoflurane and transcardially perfused with ice-cold phosphate buffered saline (PBS) followed by 4% paraformaldehyde (PFA) solution in PBS. Brains were dissected and stored overnight in 4% PFA and transferred to a 30% sucrose solution until tissue density reached equilibrium and brains sank to the bottom of their holding tubes. 40 μm brain sections were taken using a Leica CM3050 S cryostat (Leica Microsystem, Weitzlar, Germany). Brain sections were then washed in Tris-Buffered Saline (TBS) 3X for 10 min, followed by 30 min of block in TBS with 40% normal goat serum and 0.2% Triton X-100 (TBS+). Sections were then incubated in primary antibody diluted 1:500 in TBS + overnight at room temperature with gentle agitation. The next day, sections were rinsed 3X in TBS + then incubated in fluorescent secondary antibody diluted 1:1000 in TBS + at room temperature for 2–3 h with gentle agitation. Tissue was rinsed 3X with TBS, stained with DAPI, and mounted on slides in 0.15% porcine gelatin and allowed to dry in the dark overnight. Slides were then coverslipped with DPX mountant and imaged at 20X on a Zeiss LSM880 Airyscan Confocal Microscope or Nikon AX R confocal microscope. Quantification of cell marker overlap with GFAP-Cre-mCherry construct was conducted manually using the Colocalization plugin in Fiji (Version 2.9.0).

QUANTIFICATION AND STATISTICAL ANALYSIS

Statistics—Electrophysiological data was initially analyzed using ClampFit 10 software (Molecular Devices, San Jose, CA). Ca^{2+} imaging data was collected and videos were analyzed for changes in bulk astrocyte fluorescence at the target site using Inscopix Data Processing Software (Inscopix Inc., Mountain View, CA) and $\Delta F/F_{baseline}$ was calculated relative to the 30 s baseline. Datasets were organized and quantified in Microsoft Excel and then transferred to GraphPad Prism 7 for generation of graphs and statistical analyses. For analysis of two groups, an unpaired or paired Student's t test was used, unless variance between groups was found to be significantly different as determined by an F test for equal variances, in which case a non-parametric Mann-Whitney U test was used. For analysis of three or more groups across a single independent variable, a one-way ANOVA was used with a Holm-Sidak posthoc multiple comparisons test between groups as noted in the figure legends. For analysis between two or more groups across two or more independent variables, a two-way ANOVA was used with a Holm-Sidak posthoc multiple comparisons test between groups as noted in the figure legends. Area under the curve data was quantified using the AUC calculation in Graphpad Prism 7. ROUT outlier test was applied to all individual datasets with a Q = 1%. When multiple measures were taken from an identified outlier, measures were treated independently and the corresponding cell was removed from only from that dataset. Sample sizes were derived empirically and based on our previous experience with these assays. Significance was determined as $p < 0.05$ in all datasets. Data are represented as mean ± SEM excepted paired data showing individual values.

Supplementary Material

Refer to Web version on PubMed Central for supplementary material.

ACKNOWLEDGMENTS

These studies were supported by NIH grants MH107435 (S.P.), MH119817 (S.P.), and F31MH126460 (V.K.). The *Cnr1* floxed mouse generation was supported by the Integrative Neuroscience Initiative on Alcoholism (INIA stress) grant AA9013514 (E.D.). Confocal imaging for histology was performed in part through the use of the Vanderbilt Cell Imaging Shared Resource (supported by NIH grants CA68485, DK20593, DK58404, DK59637, and EY08126) and the Northwestern University Center for Advanced Microscopy generously supported by NCI CCSG P30 CA060553 awarded to the Robert H. Lurie Comprehensive Cancer Center. The graphical abstract and schematic in Figure 3B were created with BioRender.com.

REFERENCES

1. Hu H, Cui Y, and Yang Y (2020). Circuits and functions of the lateral habenula in health and in disease. Nat. Rev. Neurosci 21, 277–295. 10.1038/s41583-020-0292-4. [PubMed: 32269316]
2. Gold PW, and Kadriu B (2019). A major role for the lateral habenula in depressive illness: physiologic and molecular mechanisms. Front. Psychiatry 10, 320. 10.3389/fpsyt.2019.00320. [PubMed: 31231247]
3. Kano M, Ohno-Shosaku T, Hashimotodani Y, Uchigashima M, and Watanabe M (2009). Endocannabinoid-mediated control of synaptic transmission. Physiol. Rev 89, 309–380. 10.1152/physrev.00019.2008. [PubMed: 19126760]
4. Bedse G, Hill MN, and Patel S (2020). 2-Arachidonoylglycerol modulation of anxiety and stress adaptation: from grass roots to novel therapeutics. Biol. Psychiatry 88, 520–530. 10.1016/j.biopsych.2020.01.015. [PubMed: 32197779]
5. Berger AL, Henricks AM, Lugo JM, Wright HR, Warrick CR, Sticht MA, Morena M, Bonilla I, Laredo SA, Craft RM, et al. (2018). The lateral habenula directs coping styles under conditions of stress via recruitment of the endocannabinoid system. Biol. Psychiatry 84, 611–623. 10.1016/j.biopsych.2018.04.018. [PubMed: 29887035]
6. Shonesy BC, Bluett RJ, Ramikie TS, Báldi R, Hermanson DJ, Kingsley PJ, Marnett LJ, Winder DG, Colbran RJ, and Patel S (2014). Genetic disruption of 2-arachidonoylglycerol synthesis reveals a key role for endocannabinoid signaling in anxiety modulation. Cell Rep. 9, 1644–1653. 10.1016/j.celrep.2014.11.001. [PubMed: 25466252]
7. Patel S, and Hillard CJ (2006). Pharmacological evaluation of cannabinoid receptor ligands in a mouse model of anxiety: further evidence for an anxiolytic role for endogenous cannabinoid signaling. J. Pharmacol. Exp. Ther 318, 304–311. 10.1124/jpet.106.101287. [PubMed: 16569753]
8. Marcus DJ, Bedse G, Gaulden AD, Ryan JD, Kondev V, Winters ND, Rosas-Vidal LE, Altemus M, Mackie K, Lee FS, et al. (2020). Endocannabinoid signaling collapse mediates stress-induced amygdalo-cortical strengthening. Neuron 105, 1062–1076.e6. 10.1016/j.neuron.2019.12.024. [PubMed: 31948734]
9. Bluett RJ, Báldi R, Haymer A, Gaulden AD, Hartley ND, Parrish WP, Baechle J, Marcus DJ, Mardam-Bey R, Shonesy BC, et al. (2017). Endocannabinoid signalling modulates susceptibility to traumatic stress exposure. Nat. Commun 8, 14782. 10.1038/ncomms14782. [PubMed: 28348378]
10. Authement ME, Langlois LD, Shepard RD, Browne CA, Lucki I, Kassis H, and Nugent FS (2018). A role for corticotropin-releasing factor signaling in the lateral habenula and its modulation by early-life stress. Sci. Signal 11, eaan6480. 10.1126/scisignal.aan6480. [PubMed: 29511121]
11. Valentinova K, and Mameli M (2016). mGluR-LTD at excitatory and inhibitory synapses in the lateral habenula tunes neuronal output. Cell Rep. 16, 2298–2307. 10.1016/j.celrep.2016.07.064. [PubMed: 27545888]
12. Blum K, Khalsa J, Cadet JL, Baron D, Bowirrat A, Boyett B, Lott L, Brewer R, Gondré-Lewis M, Bunt G, et al. (2021). Cannabis-induced hypodopaminergic anhedonia and cognitive decline in humans: embracing putative induction of dopamine homeostasis. Front. Psychiatry 12, 623403. 10.3389/fpsyt.2021.623403. [PubMed: 33868044]

13. Sharpe L, Sinclair J, Kramer A, de Manincor M, and Sarris J (2020). Cannabis, a cause for anxiety? A critical appraisal of the anxiogenic and anxiolytic properties. J. Transl. Med 18, 374. 10.1186/s12967-020-02518-2. [PubMed: 33008420]

14. Patel S, Hill MN, and Hillard CJ (2014). Effects of phytocannabinoids on anxiety, mood, and the endocrine system. In Handbook of Cannabis, Pertwee R, ed. (Oxford Press), pp. 189–207. 10.1093/acprof:oso/9780199662685.003.0010.

15. Li W, Zuo W, Wu W, Zuo QK, Fu R, Wu L, Zhang H, Ndukwe M, and Ye JH (2019). Activation of glycine receptors in the lateral habenula rescues anxiety- and depression-like behaviors associated with alcohol withdrawal and reduces alcohol intake in rats. Neuropharmacology 157, 107688. 10.1016/j.neuropharm.2019.107688. [PubMed: 31254534]

16. Xie Z, Li G, and Ye JH (2013). Acute effects of ethanol on GABAA and glycine currents in the lateral habenula neurons of young rats. Open J. Neurosci 3, 5. 10.13055/ojns_3_1_5.130821. [PubMed: 28066680]

17. Park H, Rhee J, Lee S, and Chung C (2017). Selectively impaired endocannabinoid-dependent long-term depression in the lateral habenula in an animal model of depression. Cell Rep. 20, 289–296. 10.1016/j.celrep.2017.06.049. [PubMed: 28700932]

18. Wilson RI, and Nicoll RA (2001). Endogenous cannabinoids mediate retrograde signalling at hippocampal synapses. Nature 410, 588–592. 10.1038/35069076. [PubMed: 11279497]

19. Barker DJ, Miranda-Barrientos J, Zhang S, Root DH, Wang HL, Liu B, Calipari ES, and Morales M (2017). Lateral preoptic control of the lateral habenula through convergent glutamate and GABA transmission. Cell Rep. 21, 1757–1769. 10.1016/j.celrep.2017.10.066. [PubMed: 29141211]

20. Waung MW, Maanum KA, Cirino TJ, Driscoll JR, O'Brien C, Bryant S, Mansourian KA, Morales M, Barker DJ, and Margolis EB (2022). A diencephalic circuit in rats for opioid analgesia but not positive reinforcement. Nat. Commun 13, 764. 10.1038/s41467-022-28332-6. [PubMed: 35140231]

21. Shabel SJ, Proulx CD, Piriz J, and Malinow R (2014). GABA/glutamate co-release controls habenula output and is modified by antidepressant treatment. Science 345, 1494–1498. 10.1126/science.1250469. [PubMed: 25237099]

22. Wallace ML, Saunders A, Huang KW, Philson AC, Goldman M, Macosko EZ, McCarroll SA, and Sabatini BL (2017). Genetically distinct parallel pathways in the entopeduncular nucleus for limbic and sensorimotor output of the basal ganglia. Neuron 94, 138–152.e5. 10.1016/j.neuron.2017.03.017. [PubMed: 28384468]

23. Martin-Fernandez M, Jamison S, Robin LM, Zhao Z, Martin ED, Aguilar J, Benneyworth MA, Marsicano G, and Araque A (2017). Synapse-specific astrocyte gating of amygdala-related behavior. Nat. Neurosci 20, 1540–1548. 10.1038/nn.4649. [PubMed: 28945222]

24. Navarrete M, and Araque A (2008). Endocannabinoids mediate neuron-astrocyte communication. Neuron 57, 883–893. 10.1016/j.neuron.2008.01.029. [PubMed: 18367089]

25. Navarrete M, and Araque A (2010). Endocannabinoids potentiate synaptic transmission through stimulation of astrocytes. Neuron 68, 113–126. 10.1016/j.neuron.2010.08.043. [PubMed: 20920795]

26. Hablitz LM, Gunesch AN, Cravetchi O, Moldavan M, and Allen CN (2020). Cannabinoid signaling recruits astrocytes to modulate presynaptic function in the suprachiasmatic nucleus. eNeuro 7, ENEURO.0081–19. 2020. 10.1523/ENEURO.0081-19.2020.

27. Kovács A, Bordás C, Bíró T, Hegyi Z, Antal M, Szücs P, and Pál B (2017). Direct presynaptic and indirect astrocyte-mediated mechanisms both contribute to endocannabinoid signaling in the pedunculopontine nucleus of mice. Brain Struct. Funct 222, 247–266. 10.1007/s00429-016-1214-0. [PubMed: 27169390]

28. Kondev V, Morgan A, Najeed M, Winters ND, Kingsley PJ, Marnett L, and Patel S (2022). The endocannabinoid 2-arachidonoylglycerol bidirectionally modulates acute and protracted effects of predator odor exposure. Biol. Psychiatry 10.1016/j.biopsych.2022.05.012.

29. Cong J, Lu K, Zou W, Li Z, Guo Z, Tong X, Zheng J, Zhu J, Li S, Zhang W, et al. (2021). Astroglial CB1 cannabinoid receptors mediate CP 55,940-induced conditioned place

aversion through cyclooxygenase-2 signaling in mice. Front. Cell. Neurosci 15, 772549. 10.3389/fncel.2021.772549. [PubMed: 34887729]

30. Eraso-Pichot A, Pouvreau S, Olivera-Pinto A, Gomez-Sotres P, Skupio U, and Marsicano G (2023). Endocannabinoid signaling in astrocytes. Glia 71, 44–59. 10.1002/glia.24246. [PubMed: 35822691]
31. Serrat R, Covelo A, Kouskoff V, Delcasso S, Ruiz-Calvo A, Chenouard N, Stella C, Blancard C, Salin B, Julio-Kalajzić F, et al. (2021). Astroglial ER-mitochondria calcium transfer mediates endocanna-binoid-dependent synaptic integration. Cell Rep. 37, 110133. 10.1016/j.celrep.2021.110133. [PubMed: 34936875]
32. Lines J, Covelo A, Gómez R, Liu L, and Araque A (2017). Synapse-specific regulation revealed at single synapses is concealed when recording multiple synapses. Front. Cell. Neurosci 11, 367. 10.3389/fncel.2017.00367. [PubMed: 29218000]
33. Guzikowski NJ, and Kavalali ET (2021). Nano-organization at the synapse: segregation of distinct forms of neurotransmission. Front. Synaptic Neurosci 13, 796498. 10.3389/fnsyn.2021.796498. [PubMed: 35002671]
34. Fu R, Tang Y, Li W, Ren Z, Li D, Zheng J, Zuo W, Chen X, Zuo QK, Tam KL, et al. (2021). Endocannabinoid signaling in the lateral habenula regulates pain and alcohol consumption. Transl. Psychiatry 11, 220. 10.1038/s41398-021-01337-3. [PubMed: 33854035]
35. Winters ND, Bedse G, Astafyev AA, Patrick TA, Altemus M, Morgan AJ, Mukerjee S, Johnson KD, Mahajan VR, Uddin MJ, et al. (2021). Targeting diacylglycerol lipase reduces alcohol consumption in preclinical models. J. Clin. Invest 10.1172/JCI146861.
36. Kang S, Li J, Bekker A, and Ye JH (2018). Rescue of glutamate transport in the lateral habenula alleviates depression- and anxiety-like behaviors in ethanol-withdrawn rats. Neuropharmacology 129, 47–56. 10.1016/j.neuropharm.2017.11.013. [PubMed: 29128307]
37. Hegyi Z, Oláh T, Kőszeghy Á, Piscitelli F, Holló K, Pál B, Csernoch L, Di Marzo V, and Antal M (2018). CB1 receptor activation induces intracellular Ca(2+) mobilization and 2-arachidonoylglycerol release in rodent spinal cord astrocytes. Sci. Rep 8, 10562. 10.1038/s41598-018-28763-6. [PubMed: 30002493]
38. Lee JH, Durand R, Gradinaru V, Zhang F, Goshen I, Kim DS, Fenno LE, Ramakrishnan C, and Deisseroth K (2010). Global and local fMRI signals driven by neurons defined optogenetically by type and wiring. Nature 465, 788–792. 10.1038/nature09108. [PubMed: 20473285]
39. Viollet C, Simon A, Tolle V, Labarthe A, Grouselle D, Loe-Mie Y, Simonneau M, Martel G, and Epelbaum J (2017). Somatostatin-IRES-cre mice: between knockout and wild-type? Front. Endocrinol 8, 131. 10.3389/fendo.2017.00131.
40. Kim U, and Chang SY (2005). Dendritic morphology, local circuitry, and intrinsic electrophysiology of neurons in the rat medial and lateral habenular nuclei of the epithalamus. J. Comp. Neurol 483, 236–250. 10.1002/cne.20410. [PubMed: 15678472]

Highlights

- Endocannabinoids bidirectionally control lateral habenula (LHb) glutamate release
- GABA release in the LHb is inhibited by endocannabinoids
- Distinct LHb inputs are differentially controlled by endocannabinoids
- Astrocyte CB_1 receptor signaling potentiates LHb glutamate release

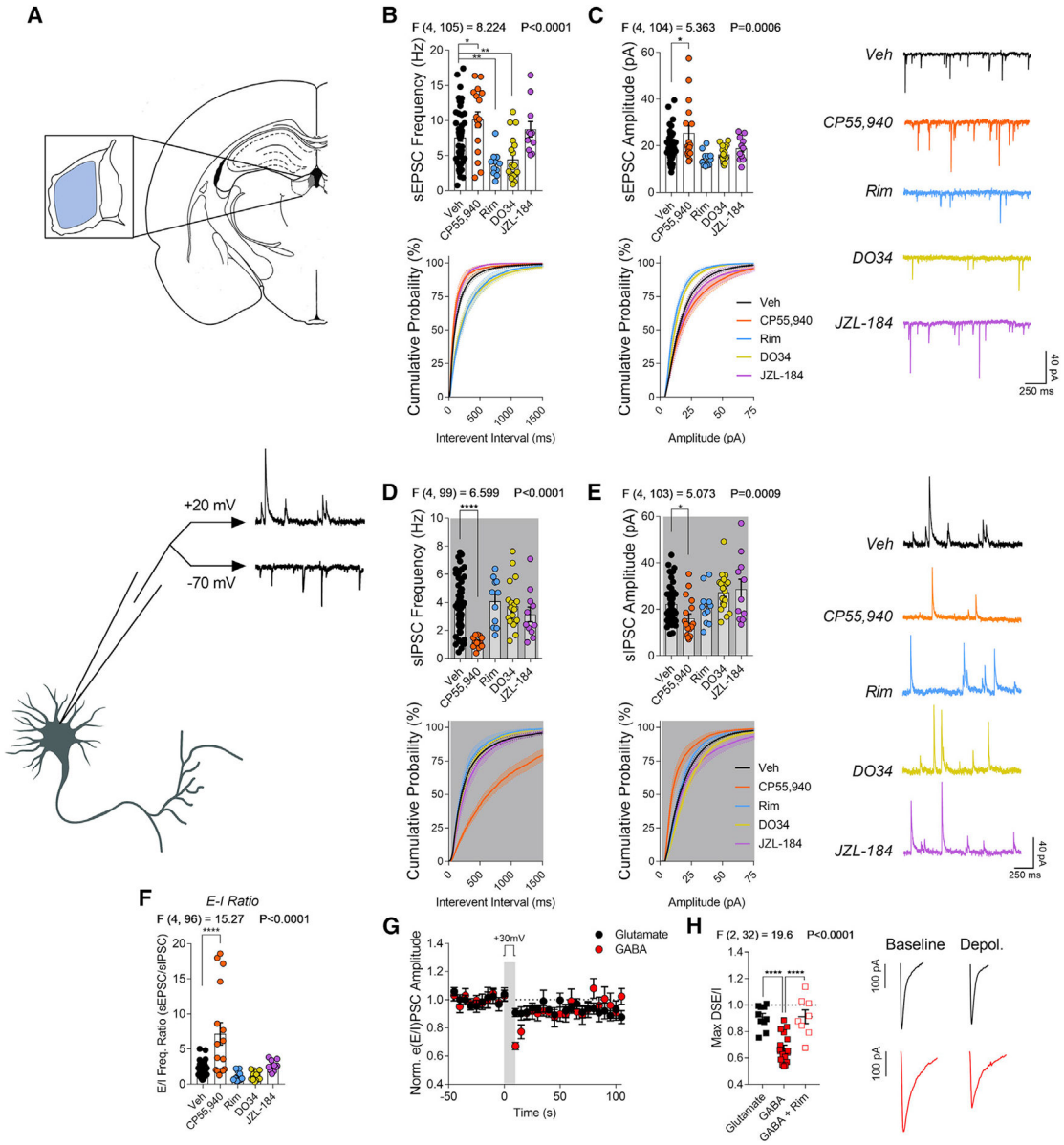

Figure 1. Endocannabinoids differentially regulate glutamatergic and GABAergic synapses in the lateral habenula

(A) Schematic of lateral habenula (LHb) recording territory and strategy for dual spontaneous excitatory/inhibitory recordings from single cells.

(B and C) Top: effects of pharmacological manipulations of the 2-AG-CB_1 system on sEPSC (B) frequency and (C) amplitude (vehicle n = 52, 18 mice; CP55,940 n = 17, 6 mice; Rim n = 11, 3 mice; DO34 n = 19/18, 5 mice; JZL-184, n = 11, 5 mice). Bottom: associated cumulative probability plots for (B) interevent interval and (C) amplitude.

(D and E) Same as (B) and (C) for sIPSCs (vehicle n = 50, 18 mice; CP55,940 n = 13/17, 6 mice; Rim n = 11, 3 mice; DO34 n = 19, 5 mice; JZL-184, n = 11, 5 mice).

(F)Same as (B)–(E) for excitation-inhibition ratio (vehicle n = 46, 18 mice; CP55,940 n = 16, 6 mice; Rimn = 10, 3 mice; DO34 n = 19/18, 5 mice; JZL-184, n = 11, 5 mice). (G and H) DSE (glutamate) and DSI (GABA) in LHb neurons.

(G) Time course of normalized synaptic current amplitude. Depolarization step was 10 s at +30 mV.

(H) Quantification of max DSE/DSI at the first sweep following depolarization. GABA + Rim time course in Figure S1G (glutamate n = 10, 3 mice; GABA n = 17, 7 mice; GABA + Rim n = 8, 3 mice).

Data are mean ± SEM; n = number of cells. Data are analyzed by one-way ANOVA with Holm-Sidak multiple comparisons relative to (B–F) vehicle or (H) between all groups. F and p values for ANOVA and significance for post-hoc multiple comparisons shown on relevant panels (*$p < 0.05$, **$p < 0.01$, ****$p < 0.0001$).

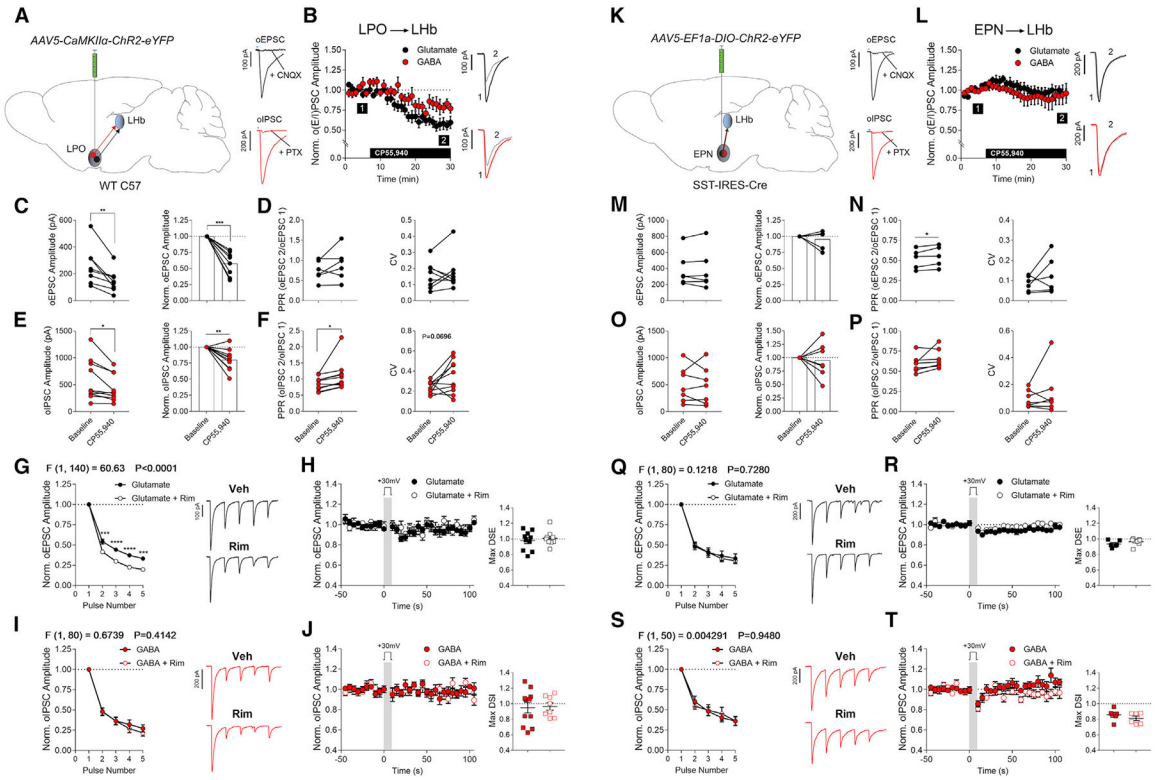

Figure 2. Distinct inputs to the LHb are differentially regulated by endocannabinoids

(A) Schematic of strategy for optogenetic study of the LPO-LHb circuit; pharmacological validation of oEPSCs and oIPSCs. CNQX, AMPA antagonist; PTX, $GABA_A$ antagonist.).

(B) Time course of CP55,940 bath application effects on oEPSC and oIPSC amplitude at LPO-LHb synapses. Time points 1 and 2 represent baseline and last 2 min of drug application, respectively (glutamate n = 8, 6 mice; GABA = 13, 7 mice).

(C–F) CP55,940 effects on LPO-LHb (C) oEPSC amplitude, (D) oEPSC PPR and CV, (E) oIPSC amplitude, and (F) oIPSC PPR and CV at baseline and post-drug application (oEPSC amplitude, CV n = 8, 6 mice; oEPSC PPR n = 6, 4 mice; oIPSC amplitude, PPR, CV n = 10, 6 mice).

(G) Rim effects on LPO-LHb oEPSC amplitude during a 250 ms 20 Hz pulse train, normalized to pulse 1 (n = 17, 4 mice).

(H) DSE at LPO-LHb synapses. Left: time course of normalized oEPSC amplitude. Depolarization step was 10 s at +30 mV. Right: quantification of max DSE at the first sweep following depolarization (glutamate n = 10, 3 mice; glutamate + Rim n = 9, 3 mice).

(I) Same as (G) for LPO-LHb oIPSCs (GABA n = 10, 4 mice; GABA + Rim n = 8, 3 mice).

(J) DSI at LPO-LHb synapses. Same as (H) for LPO-LHb oIPSCs (GABA n = 11, 4 mice; GABA + Rim n = 8, 3 mice).

(K) Same as (A) for the EPN-LHb circuit.

(L) Same as (B) for EPN-LHb oEPSC and oIPSC amplitude (glutamate n = 6, 5 mice; GABA = 7, 4 mice).

(M–P) Same as (C)–(F) for EPN-LHb oEPSCs and oIPSCs (oEPSC amplitude, CV = 6, 5 mice; oEPSC PPR n = 5, 5 mice; oIPSC amplitude, PPR, CV n = 7, 4 mice).

(Q) Same as (G) for EPN-LHb oEPSCs (glutamate n = 9, 3 mice; glutamate + Rim n = 9, 3 mice).
(R) DSE at EPN-LHb synapses. Same as (H) for EPN-LHb oEPSCs (glutamate n = 6, 3 mice; glutamate + Rim n = 8, 3 mice).
(S) Same as (G) for EPN-LHb oIPSCs (GABA n = 6, 3 mice; GABA + Rim n = 6 mice).
(T) DSI at EPN-LHb synapses. Same as (H) for EPN-LHb oIPSCs (GABA n = 6, 3 mice; GABA + Rim n = 6, 3 mice).
Data are mean ± SEM except paired data; n = number of cells. Data analyzed by (C–F and M–P) two-tailed paired t test, (G, I, Q, and S) two-way ANOVA with Holm-Sidak multiple comparisons between control and Rim, or (H, J, R, and T, right) two-tailed t test. Significance for t tests, ANOVA F and p values formain effect of drug, and significance for post-hoc multiple comparisons shown on relevant panels (*$p < 0.05$, **$p < 0.01$, ***$p < 0.001$, ****$p < 0.0001$).

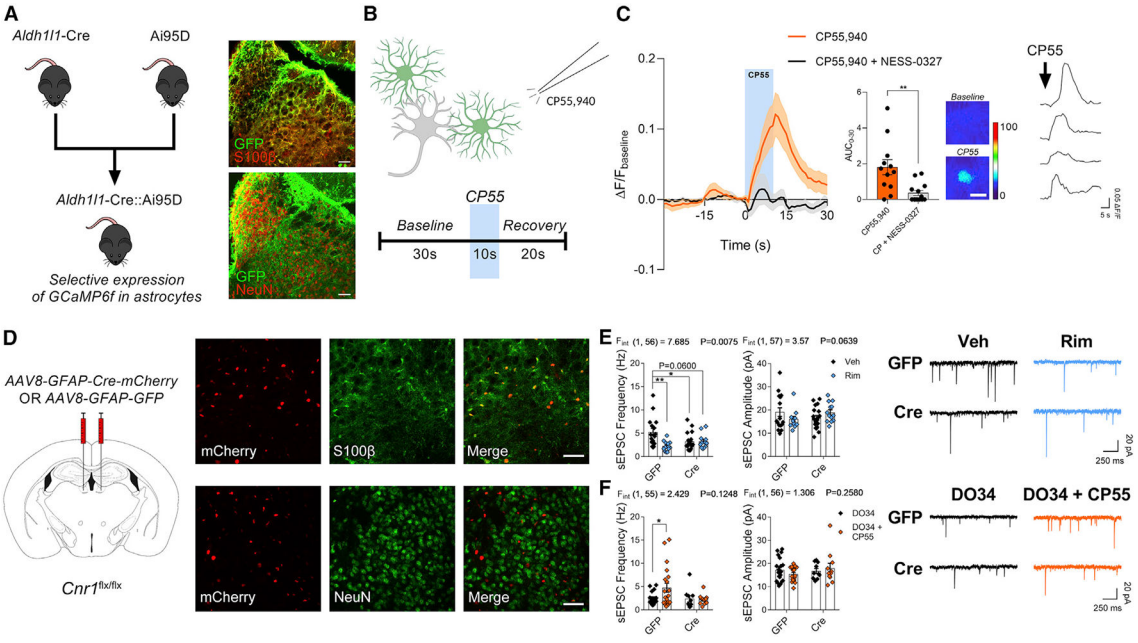

Figure 3. Astrocytic CB_1 receptors positively modulate LHb glutamate release

(A) Left: breeding scheme for Aldh1l1-Cre:Ai95D mice. Right: staining in LHb for canonical astrocyte and neuron markers against GFP staining for GCaMP6f. Scale bar: 50 μm.

(B) Schematic of experimental approach for *ex vivo* Ca^{2+} imaging in astrocytes (green).

(C) Effect of local CP55,940 application on astrocyte Ca^{2+} signals. Left: ΔF/F at drug application site and positive area under the curve (AUC) from 0 to 30 s (CP55,940 n = 12, 3 mice; CP + NESS-0327 n = 13, 3 mice). Right: widefield pseudo-colored ΔF/F-adjusted images of a pre-identified cell pre- vs. post-CP55,940 application; sample traces from individual cells. Scale bar: 10 μm.

(D) Left: schematic for viral injections in the LHb. Right: staining for canonical astrocyte and neuron markers against expression of GFAP-Cre-mCherry. Scale bar: 50 μm. See also Figure S3C.

(E) Effects of astrocytic CB_1 receptor deletion and Rim on sEPSC frequency and amplitude (GFP vehicle [Veh] n = 16/17, 5 mice; GFP Rim n = 13, 5mice; Cre Veh n = 19, 6 mice; Cre Rim = 13/14, 6 mice).

(F) Same as (E) for DO34 ± CPP55,940 effects (GFP DO34 n = 18/20, 6 mice; GFP DO34 + CP55 n = 20/19, 6 mice; Cre DO34 n = 10, 4 mice; Cre DO34 + CP55 = 11, 4 mice).

Data are mean ± SEM; n = number of cells. Data analyzed by (C) Mann-Whitney U test or (E and F) two-way ANOVA with Holm-Sidak multiple comparisons (E) between all groups or (F) between DO34 and DO34 + CP55 within each virus genotype. Significance for U test, F and p values for drug × virus interaction for ANOVA, and significance for post-hoc multiple comparisons shown on relevant panels (*p < 0.05, **p < 0.01).

KEY RESOURCES TABLE

REAGENT or RESOURCE	SOURCE	IDENTIFIER
Antibodies		
Rabbit α-s100β	Abcam	Cat. #: ab52642; RRID: AB_882426
Rabbit α-NeuN	Millipore	Cat. #: ABN78; RRID: AB_10807945
Chicken α-GFP	Abcam	Cat. #: ab13970; RRID: AB_300798
Alexa Fluor 488 Donkey-α-Rabbit	Abcam	Cat. #: ab150073; RRID: AB_2636877
Cy5 Donkey-α-Rabbit	Jackson Immuno	Cat. #: 711-175-152; RRID: AB_2340607
Cy2 Donkey-α-Chicken	Jackson Immuno	Cat. #: 703-225-155; RRID: AB_2340370
Bacterial and virus strains		
AAV8-GFAP-Cre-mCherry	UNC Vector Core	N/A
AAV8-GFAP-GFP	UNC Vector Core	N/A
AAV5-CaMKIIa-hChR2(H134R)-EYFP	(Lee et al., 2010)[38]	RRID: Addgene_26969
AAV5-EF1a-DIO-hChR2(H134R)-EYFP-WPRE	Gift from Karl Deisseroth	RRID:Addgene_20298
AAV9-hSyn-eGFP-Cre	Gift from James M. Wilson	RRID:Addgene_105540
Chemicals, peptides, and recombinant proteins		
CP55,940	Cayman Chemical	Cat. #: 13241
Rimonabant	Cayman Chemical	Cat. #: 9000484
DO34	Glixx Laboratories	Cat. #: GLXC-09757
JZL184	Cayman Chemical	Cat. #: 13158
NESS-0327	Cayman Chemical	Cat. #: 10004184
Experimental models: Organisms/strains		
Cnr1$^{flx/flx}$ mice	(Marcus et al., 2020)[8]	N/A
Aldh1l1-Cre/ERT2 mice	Jackson Laboratory	RRID IMSR_JAX:031008
Ai95D mice	Jackson Laboratory	RRID IMSR_JAX:028865
C57 WT mice	Jackson Laboratory	RRID IMSR_JAX:000664
SOM-IRES-Cre mice	Jackson Laboratory	RRID IMSR_JAX:013044
Ai14 mice	Jackson Laboratory	RRID IMSR_JAX:007914
Software and algorithms		
Prism 7	GraphPad	https://www.graphpad.com
pClamp 10	Molecular Devices	https://www.moleculardevices.com
Inscopix Data Processing Software	Inscopix	https://www.inscopix.com/
ImageJ/FIJI	NIH	https://imagej.nih.gov/ij/